Journal of Power Sources 264 (2014) 161–167

Contents lists available at ScienceDirect

Journal of Power Sources

journal homepage: www.elsevier.com/locate/jpowsour

Short communication

Synthesis of hierarchical porous NiO nanotube arrays for supercapacitor application

F. Cao [a,*], G.X. Pan [a], X.H. Xia [b], P.S. Tang [a], H.F. Chen [a]

[a] Department of Chemistry, Huzhou Teachers College, Huzhou, 313000, China
[b] Division of Physics and Applied Physics, School of Physical and Mathematical Sciences, Nanyang Technological University, Singapore 637371, Singapore

HIGHLIGHTS

- Construct a hierarchical porous NiO nanotube array.
- Porous nanotube array shows high pseudo-capacitive properties.
- Porous nanotube array structure is favorable for fast ion and electron transfer.

GRAPHICAL ABSTRACT

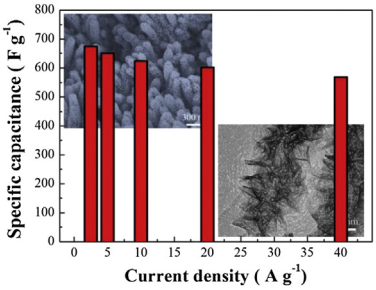

ARTICLE INFO

Article history:
Received 9 March 2014
Received in revised form
10 April 2014
Accepted 17 April 2014
Available online 30 April 2014

Keywords:
Nanotube
Electrodeposition
Nickel oxide
Porous materials
Supercapacitors

ABSTRACT

Tailor-made porous nanotube arrays are of great technological interest for the development of high-performance optical and electrochemical energy storage devices. Herein, we report facile successive electro-deposition (ED) methods to fabricate three-dimensional (3D) hierarchical porous NiO nanotube arrays on nickel foam with the help of ZnO nanorod template. The obtained hierarchical porous NiO nanotubes have a diameter of ~170 nm and consist of interconnected branch nanoflakes of ~10 nm. The resulting NiO nanotube arrays are well characterized as positive electrode materials for supercapacitor application by cyclic voltammetry (CV) and galvanostatic charge/discharge measurements. Due to the unique architecture, the NiO nanotube arrays exhibit a high capacitance of 675 F g^{-1} at the 2 A g^{-1} and 569 F g^{-1} at 40 A g^{-1}, respectively, as well as good cycling stability. The proposed synthesis method is expected for fabrication of other nanotube arrays for applications in solar cells, gas sensors and Li ion batteries.

1. Introduction

Over the past decades, there has been great interest in developing and refining more efficient energy storage devices [1–4]. Among various power sources, supercapacitor is a mature technology and has the potential of significantly advancing the energy storage market. Despite the great progress in research, supercapacitors still suffer from low energy density (only a fraction of lithium ion batteries), which prevents them from commercialization in many important fields [5,6]. It is therefore highly desirable, and has been under current research focus, to develop supercapacitors with both high energy and power densities to enable their use as primary power sources.

The performance of supercapacitors, both electric double layer capacitors (EDLCs) and pseudo-capacitors, is mainly determined by the electrode material, which is the core part of the supercapacitors and the key to high performance [1]. EDLCs, the most common and commercially available devices, use

* Corresponding author. Tel.: +86 572 232 1166.
E-mail addresses: caofenghz@126.com, helloxiaxinhui@hotmail.com (F. Cao).

http://dx.doi.org/10.1016/j.jpowsour.2014.04.103
0378-7753/

carbon-based active materials with high surface areas [7–9]. Though carbon materials are very stale and show excellent cycle life, they are beset with relatively low specific capacitance (<300 F g^{-1}) and instability at super high charge/discharge rates [5]. In recent years, the research on high-capacitance supercapacitors focuses on pseudo-capacitors which have significantly higher capacitances (several times larger than EDLCs) and energy densities arising from faradic redox reactions. The explored pseudo-capacitive materials include conducting polymers [10,11], metal oxides/hydroxides [12–18], metal sulfides [19], binary metal oxides/hydroxides [20–22]. Among the explored materials, NiO is considered as one of the most promising pseudo-capacitive electrode materials due to its high capacitance and excellent electrochemical reaction reactivity [23]. However, the practical utilization of NiO is still low resulting in low capacitance owing to the fact that the NiO has drawbacks of poor conductivity, which is kinetically unfavorable to support fast electron/ion transport required by high power density. One of solutions is to achieve rational-designed nanostructures of the NiO materials. The energy density and power density of the NiO materials are controlled by the intrinsic electrochemical activity of NiO, and kinetics of charges and ions of the electrode. Therefore, it is crucial to enhance the kinetics of ion and electron transport in NiO electrodes and at the electrode/electrolyte interface to improve reactivity and power density. To date, several strategies have been undertaken to enhance the reactivity and kinetics features of the NiO electrode materials. One way is direct growth of NiO nano-materials (such as nanowires [24], nanoflakes [25], nanosheets [26], bowl-like films [27], nanowalls [28], nanoparticles [29]) on current collectors. This integrated electrode ensures a good electric connection of the active material to the current collector without the necessity of polymer binder or conductive additives. Moreover, the nano-arrays are generally characterized by a highly porous structure in the form of nanotubes, nanowires, nanorods or random nanoporous structures. These nanoscale porous architectures provide fast ion/electron transfer, large reaction surface area and good strain accommodation leading to enhanced performance [30,31].

In the present work, we report self-supported hierarchical porous NiO nanotube arrays grown on nickel foam and demonstrate their noticeable supercapacitor performance. Different from previous NiO-based electrode materials, we develop successive electro-deposition (ED) methods to prepare porous NiO nanotube arrays by the aid of ED-ZnO nanorod arrays. The NiO nanotube arrays are made up of interconnected nanoflakes. As a positive electrode material for supercapacitors, the porous NiO nanotube arrays show remarkable supercapacitor performance with a high capacitance of 675 F g^{-1} at 2 A g^{-1} as well as high cycle life. It is

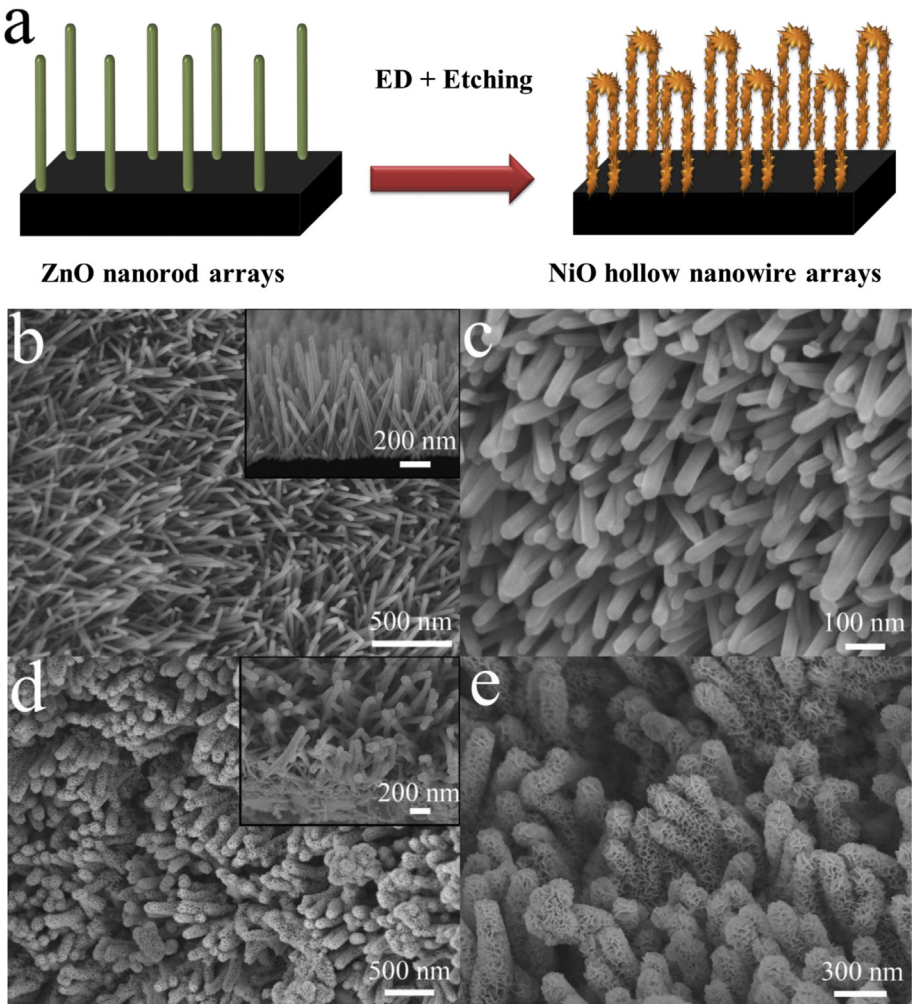

Fig. 1. (a) Schematic illustration of ED-synthesis of hierarchical porous NiO nanotube arrays. SEM images of (b, c) ZnO nanorod arrays, and (d, e) hierarchical porous NiO nanotube arrays.

expected that the developed synthetic method can be applicable for the synthesis of other advanced nanotube nanoarrays for electrochemical energy storage devices.

2. Experimental

Synthesis of the hierarchical porous NiO nanotube arrays was schematically illustrated in Fig. 1a. The hierarchical porous NiO nanotube arrays were prepared by successive electro-deposition (ED) methods with the help of ZnO nanorod template. First, ZnO nanorod arrays were electrodeposited in solution of 0.01 M $Zn(NO_3)_2$ + 0.05 M NH_4NO_3 with current density of 0.25 mA cm^{-2} at 70 °C for 45 min in a three-compartment system, the nickel foam (Alantum Advanced Technology Materials (Shenyang), a 280 g m^{-2} in areal density, a porosity of 99.5% and 1.0 mm in thickness) as the working substrate, saturated calomel electrode (SCE) as the reference electrode and a Pt foil as the counter-electrode. Then, the self-supported ZnO nanorod arrays were used as the scaffold for NiO nanoflake shell growth via a simple ED method. The electrolyte consisted of 0.13 M nickel sulfate, 0.13 M Na_2SO_4 and 0.1 M sodium acetate. The ED experiment was carried out at a constant anodic current of 0.25 mA cm^{-2} for 1 h. Then, the samples were immersed in 0.5 M NaOH for 30 min to remove the ZnO template. Finally, the samples were rinsed with distilled water and annealed at 350 °C in argon for 1.5 h to form porous NiO nanotube arrays. The involved growth reactions of the NiO were briefly proposed as follows [25,32].

$$\text{Precursor reaction}: \quad Ni^{2+} - e^- + 3OH^- \rightarrow NiOOH \cdot H_2O \tag{1}$$

$$\text{During annealing process}: \quad NiOOH \cdot H_2O - e^- \rightarrow Ni(OH)_2 + OH^- \tag{2}$$

$$Ni(OH)_2 \rightarrow NiO + H_2O \tag{3}$$

The morphologies and structures of the as-synthesized samples were characterized by X-ray diffraction (XRD, RIGAKU D/Max-2550 with Cu K radiation), field emission scanning electron microscopy (FESEM, FEI SIRION), transmission electron microscopy (TEM, JEOL JEM200CX), high-resolution transmission electron microscopy (HRTEM, JEOL JEM-2010F), and X-ray photoelectron spectroscopy (XPS, PHI 5700). The surface area of the sample that scratched from the substrate was determined by BET measurements using a NOVA-1000e surface area analyzer.

The load weight of the NiO nanotube arrays is ~1.2 mg cm^{-2}. The length of the NiO nanotube arrays is ~1.1 μm. The electrochemical measurements were carried out in a three-electrode electrochemical cell containing 2 M KOH aqueous solution as the electrolyte. The porous NiO nanotube arrays were used as the

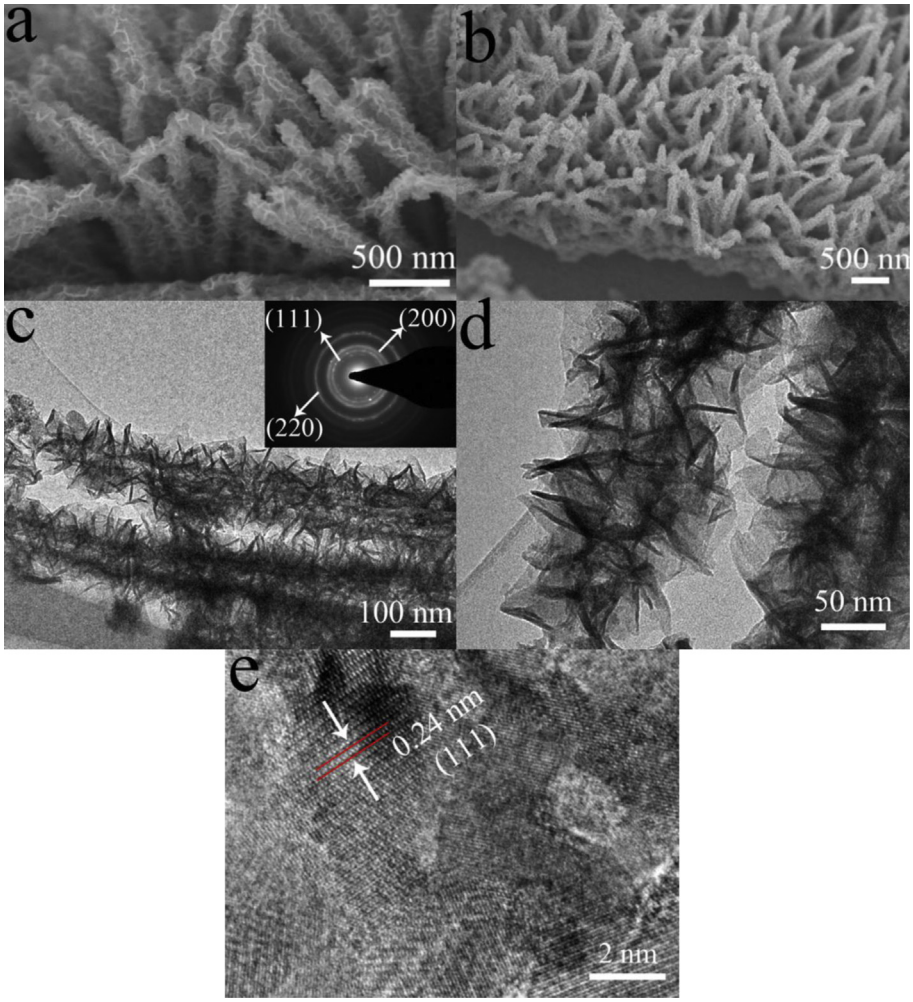

Fig. 2. (a, b) Cross-sectional SEM images of porous NiO nanotube arrays on nickel foam. TEM-HETRM images of (c–e) hierarchical porous NiO nanotube (SAED pattern in inset).

working electrode, Hg/HgO as the reference electrode and a Pt foil as the counter-electrode. A series of electrochemical tests including cyclic voltammetry (CV), and galvanostatic charge/discharge measurements were performed on CHI660c electrochemical workstation (Chenhua, Shanghai) and Xinwei supercapacitor program-control test system. The specific capacitance was calculated according to the following equation [1,6]:

$$C = \frac{I\Delta t}{M\Delta V} \tag{4}$$

where C (F g^{-1}) was specific capacitance, I (mA) represented discharge current, and M (mg), ΔV (V) and Δt (s) designated mass of active materials, potential drop during discharge and total discharge time, respectively.

3. Results and discussion

SEM images of the ZnO nanorod arrays are shown in Fig. 1b and c. The electrodeposited ZnO nanorod has an average diameter of 60 nm, length up to around 1 μm (Fig. 1b and c). After electrodeposition of NiO and etching the ZnO template, free-standing NiO nanotubes composed of nanoflakes of ~10 nm thick are left on the nickel foam substrate (Fig. 1d and e). The NiO nanoflake shells are interconnected with each other forming hierarchical porosity. The average diameter of the porous NiO nanotubes is ~170 nm. The cross-sectional SEM images of the NiO nanotube are shown in Fig. 2a and b. Obviously, the NiO nanotube has a tight connection with the nickel foam substrate. Also observe that the length of the NiO nanotube is about 1.1 μm. The detailed structure of the porous NiO nanotube is analyzed by TEM-HRTEM (Fig. 2c–e). After decoration of NiO and etching the ZnO template, the hierarchical porous NiO nanotube can be easily distinguished from the TEM images (Fig. 2c and d). It is indicated that the porous NiO nanotubes consist of interconnected NiO nanoflakes and show a hollow center. In addition, the nanoflake shell (Fig. 2c) shows a polycrystalline SAED pattern corresponding to cubic NiO phase (JCPDS 4-0835). Furthermore, the measured lattice spacing of 0.24 nm is in good agreement with the (111) interplanar distance of the NiO phase (Fig. 2e).

The formation of the porous NiO nanotubes is also verified by X-ray diffraction (XRD) and X-ray photoelectron spectroscopy (XPS) analysis. In addition to the three typical diffraction peaks from the nickel foam, for the ZnO nanorod template, the XRD pattern contains characteristic peaks of hexagonal ZnO phase (JCPDS 36-1451). After ED of NiO and etching the ZnO template, the diffraction peaks of ZnO disappear and new peaks of cubic NiO phase (JCPDS 4-0835) are observed (Fig. 3a), which is also supported by XPS results. For the Ni 2p spectra (Fig. 3b), two Ni 2p core levels ($2p_{1/2}$ and $2p_{3/2}$) and two satellite peaks are observed. The binding energy separation between core levels Ni $2p_{1/2}$ (873.5 eV) and Ni $2p_{3/2}$ (855.9 eV) is ~17.6 eV, which matches with electronic states of NiO [33]. In O1s spectra (Fig. 3c), the peak at 530.5 eV reveals the existence of Ni–O bond, which is consistent with NiO electronic state [33]. Based on the results above, it is reasonable that the hierarchical porous NiO nanotube arrays are successfully prepared by the successive ED methods with the help of sacrificial ZnO nanorod template. Because of the porous structure, the porous NiO nanotubes exhibit a large surface area of ~165 m^2 g^{-1} (Fig. 3d) and the pore size distribution of the NiO nanotube shows peaks at 75 and 135 nm, respectively. The large surface area is favorable for enhancing the electrolyte–material contact area and providing large reactive reaction area [34,35]. In our case, the sheet resistance of the porous NiO nanotube powder from the substrate is about 1200 Ω/square, measured by four points probe technique.

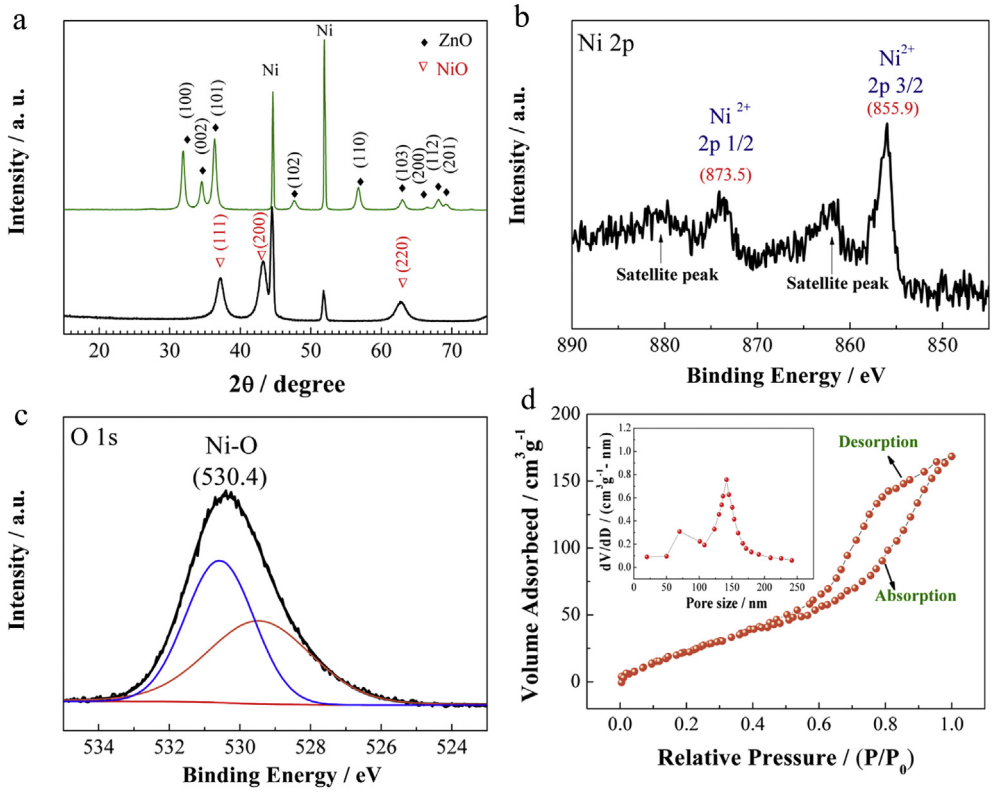

Fig. 3. (a) XRD patterns of ZnO nanorod and porous NiO nanotube arrays on nickel foams. XPS spectra of porous NiO nanotube: (b) Ni 2p and (c) O 1s. (d) BET measurement of porous NiO nanotubes (pore distribution in inset).

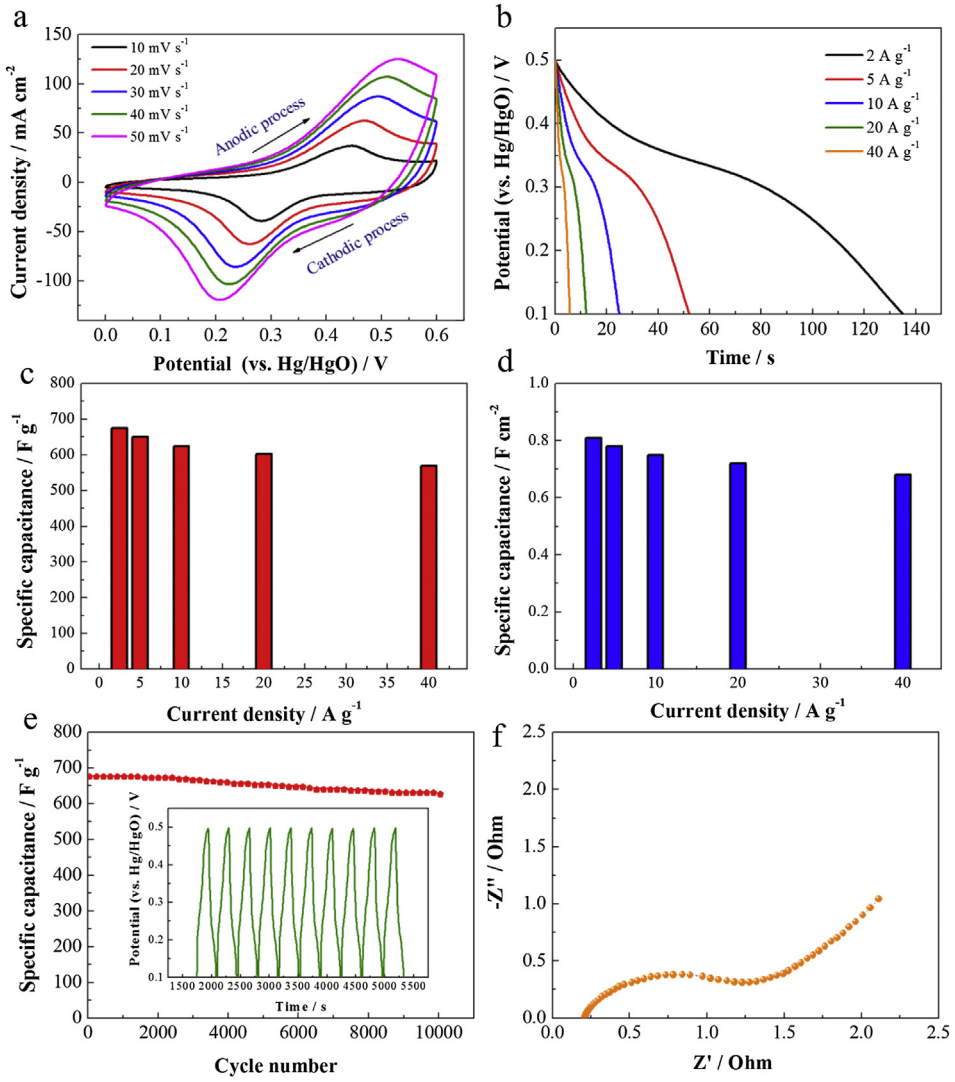

Fig. 4. Electrochemical and structural characterizations of porous NiO nanotube arrays: (a) CV curves at different scanning rates. (b) Discharge curves at different current densities and (c) corresponding specific capacitances at different current densities. (d) Typical areal capacitance of porous NiO nanotube arrays at different current densities. (e) Cycling performance at 2 A g^{-1} (typical charge/discharge curves in inset). (f) Nyquist plot of porous NiO nanotube arrays at discharge state after 10,000 cycles.

Supercapacitor properties of the porous NiO nanotube arrays are elucidated by cyclic voltammograms (CV) and galvanostatic charge/discharge tests. Fig. 4a shows the typical CV curves of porous NiO nanotube arrays at different scanning rates. One obvious redox reaction is observed in the CV curve and this electrochemical reaction is due to the conversion between NiO and NiOOH, simply expressed as follows [26,32,36].

$$NiO - e^- + OH^- \rightarrow NiOOH \quad (5)$$

The charge process is associated with the oxidation peak to store energy, whereas the discharge process is associated with the reduction peak to release energy. Galvanostatic discharge curves of the porous NiO nanotube arrays at various current densities, and corresponding specific capacitances versus discharge current densities are presented in Fig. 4b and c. The calculated specific capacitance of the porous NiO nanotube arrays is 675 F g^{-1} at 2 A g^{-1}, 650 F g^{-1} at 5 A g^{-1}, 624 F g^{-1} at 10 A g^{-1}, 603 F g^{-1} at 20 A g^{-1}, 569 F g^{-1} at 40 A g^{-1}, respectively. A high capacitance retention of 84% is retained when the charge/discharge rate changes from 2 A g^{-1} to 40 A g^{-1}. These obtained capacitance values are higher than other NiO films (such as nanoflake film [25,37], nanosheet [38,39], and nano-triangle film [40]) and NiO powders [41], and comparable to self-supporting Co_3O_4 nanowires (600–746 F g^{-1}) [12,42], but lower than the CNT-NiO nanotubes (~903 F g^{-1}) [43]. The discharge areal capacitance of the NiO nanotube arrays is measured to be 0.8 F cm^{-2} at 2 A g^{-1} (Fig. 4d), which is larger than the Co_3O_4 nanowire arrays (0.68 F cm^{-2}) and common NiO nanoflake arrays (0.25 F cm^{-2}) [31]. We further studied the cycling performance of the porous NiO nanotube arrays at 2 A g^{-1} (Fig. 4e). The porous NiO nanotube arrays exhibit excellent capacitance retention with 629 F g^{-1} after 10,000 cycles maintaining 93.2% of the maximum value (Fig. 4e), higher than NiO nanoflake films prepared by chemical bath deposition (178 F g^{-1} after 6000 cycles), demonstrating its excellent capacitance retention. Fig. 4f shows the Nyquist plots of NiO nanotube arrays after 10,000 cycles. The Nyquist plot consists of a depressed arc in high frequency regions and an inclined line in low frequency regions. The cross point between real axis and curve indicates the total ohmic resistance between solution and electrode. After 10,000 cycles, the resistance is about 0.2 Ω, which is low and favorable for supercapacitor application. In addition, we also investigated the substrate effect on

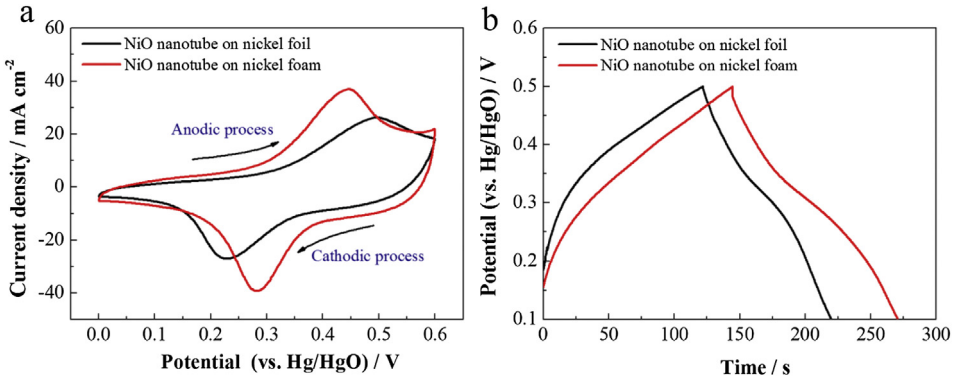

Fig. 5. Electrochemical performances of porous NiO nanotube arrays on nickel foam and nickel foil substrates: (a) CV curves at the scanning rate of 10 mV s^{-1} at 50th cycle. (b) Charge/discharge profiles at 2 A g^{-1} at 50th cycle.

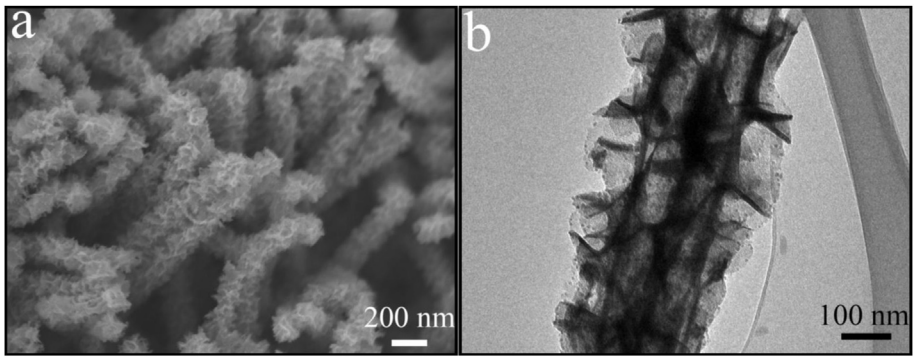

Fig. 6. (a, b) SEM–TEM images of porous NiO nanotubes after 10,000 cycles at 2 A g^{-1}.

supercapacitor performance. We compared the electrochemical performance of NiO nanotube arrays on nickel foam and nickel foil, respectively (Fig. 5). Importantly, notice that the porous NiO nanotube arrays on nickel foam show lower oxidation potentials, higher reduction potentials and higher peak current densities than the NiO nanotube arrays on nickel foil (Fig. 5a). It is indicated that the porous NiO nanotube arrays on nickel foam have better electrochemical activity and reaction reversibility. This is supported by the charge/discharge curves at 2 A g^{-1} (Fig. 5b). The specific capacitance of porous NiO nanotube arrays on nickel foam is 675 F g^{-1} at 2 A g^{-1}, higher than the NiO nanotube on the nickel foil (495 F g^{-1} at 2 A g^{-1}). Moreover, the porous NiO nanotube arrays on nickel foam exhibit much lower charge voltage plateau and higher discharge voltage plateau than the counterpart on the nickel foil, meaning that the NiO nanotube on nickel foam has smaller polarization and better performance, due to the fact that the 3D porous nickel foam substrates provide higher active surface area and inner space for fast ion/electron transfer and higher energy conversion efficiency.

The high capacitances and excellent cycling stability of the porous NiO nanotube arrays are due to the unique nanotube arrays architecture. First, nanotube arrays are directly grown on the nickel foam substrate. Such intimate binding affords facile electron transport for individual NiO nanotube. Second, this porous nanotube structure creates fast electrochemical accessibility of the electrolyte and ions to the active materials, favoring the efficient contact between active materials and the electrolytes, thus leading to fast kinetics. Third, the high surface area of 3D nanotube architecture favors the efficient contact between active materials and electrolytes, providing more active sites for electrochemical reactions. Four, strong mechanical stability can accommodate the strains caused during the reactions leading to enhanced cycling performance. The structure of the porous NiO nanotube arrays after 10,000 cycles still keep intact (Fig. 6a and b), meaning that the porous NiO nanotube arrays have a strong mechanical stability, which is beneficial for the improvement of cycling stability. All these features contribute to the high specific capacitance and cycling life of the porous NiO nanotube arrays.

4. Conclusion

In summary, we have demonstrated a facile successive ED method for the fabrication of hierarchical porous NiO nanotube arrays. The as-prepared NiO nanotubes have hierarchical porous structure composed of interconnected nanoflakes, as well as large surface area. As a positive electrode material for supercapacitor, the porous NiO nanotube arrays show high capacitance of 675 F g^{-1} at 2 A g^{-1} and a high retention of 93.2% after 10,000 cycles at 2 A g^{-1}. Its hierarchical porous architecture favors fast ion/electron transfer and provides large reaction surface area, leading to fast kinetics and high capacitance. It is also expected that this synthetic method can be extended to the synthesis of other metal oxide nanotube arrays.

References

[1] C. Liu, F. Li, L.P. Ma, H.M. Cheng, Adv. Mater. 22 (2010) E28.
[2] X.-C. Dong, H. Xu, X.-W. Wang, Y.-X. Huang, M.B. Chan-Park, H. Zhang, L.-H. Wang, W. Huang, P. Chen, ACS Nano 6 (2012) 3206.
[3] Y. Zhang, H. Feng, X.B. Wu, L.Z. Wang, A.Q. Zhang, T.C. Xia, H.C. Dong, X.F. Li, L.S. Zhang, Int. J. Hydrogen Energy 34 (2009) 4889.
[4] X. Xia, Q. Xiong, Y. Zhang, J. Tu, C.F. Ng, H.J. Fan, Small (2014), http://dx.doi.org/10.1002/smll.201303958.
[5] P. Simon, Y. Gogotsi, Nat. Mater. 7 (2008) 845.
[6] G.P. Wang, L. Zhang, J.J. Zhang, Chem. Soc. Rev. 41 (2012) 797.

[7] F.Y. Zeng, Y.F. Kuang, N.S. Zhang, Z.Y. Huang, Y. Pan, Z.H. Hou, H.H. Zhou, C.L. Yan, O.G. Schmidt, J. Power Sources 247 (2014) 396.
[8] Z.P. Zhou, X.F. Wu, J. Power Sources 222 (2013) 410.
[9] M. Yang, Y. Zhong, L. Su, J. Wei, Z. Zhou, Chem. Eur. J. (2014), http://dx.doi.org/10.1002/chem.201304805.
[10] K. Zhang, L.L. Zhang, X.S. Zhao, J. Wu, Chem. Mater. 22 (2010) 1392.
[11] A. Bahloul, B. Nessark, E. Briot, H. Groult, A. Mauger, K. Zaghib, C.M. Julien, J. Power Sources 240 (2013) 267.
[12] X.H. Xia, J.P. Tu, Y.J. Mai, X.L. Wang, C.D. Gu, X.B. Zhao, J. Mater. Chem. 21 (2011) 9319.
[13] X.H. Xia, J.P. Tu, Y.Q. Zhang, Y.J. Mai, X.L. Wang, C.D. Gu, X.B. Zhao, J. Phys. Chem. C 115 (2011) 22662.
[14] X.H. Xia, J.P. Tu, X.L. Wang, C.D. Gu, X.B. Zhao, Chem. Commun. 47 (2011) 5786.
[15] C.C. Hu, K.H. Chang, M.C. Lin, Y.T. Wu, Nano Lett. 6 (2006) 2690.
[16] M. Hakamada, A. Moriguchi, M. Mabuchi, J. Power Sources 245 (2014) 324.
[17] W. Du, R.M. Liu, Y.W. Jiang, Q.Y. Lu, Y.Z. Fan, F. Gao, J. Power Sources 227 (2013) 101.
[18] J. Li, M. Yang, J. Wei, Z. Zhou, Nanoscale 4 (2012) 4498.
[19] X. Xia, C. Zhu, J. Luo, Z. Zeng, C. Guan, C.F. Ng, H. Zhang, H.J. Fan, Small 10 (2014) 766.
[20] X.Y. Dong, L. Wang, D. Wang, C. Li, J. Jin, Langmuir 28 (2012) 293.
[21] S. Huang, G.N. Zhu, C. Zhang, W.W. Tjiu, Y.Y. Xia, T.X. Liu, ACS Appl. Mat. Interfaces 4 (2012) 2242.
[22] T.Y. Wei, C.H. Chen, H.C. Chien, S.Y. Lu, C.C. Hu, Adv. Mater. 22 (2010) 347.
[23] M. Yang, J.X. Li, H.H. Li, L.W. Su, J.P. Wei, Z. Zhou, Phys. Chem. Chem. Phys. 14 (2012) 11048.
[24] J.Y. Kim, S.H. Lee, Y.F. Yan, J. Oh, K. Zhu, RSC Adv. 2 (2012) 8281.
[25] X.H. Xia, J.P. Tu, X.L. Wang, C.D. Gu, X.B. Zhao, J. Mater. Chem. 21 (2011) 671.
[26] Z.H. Yang, F.F. Xu, W.X. Zhang, Z.S. Mei, B. Pei, X. Zhu, J. Power Sources 246 (2014) 24.
[27] M.S. Wu, M.J. Wang, J.J. Jow, J. Power Sources 195 (2010) 3950.
[28] J.H. Zhu, J.A. Jiang, J.P. Liu, R.M. Ding, H. Ding, Y.M. Feng, G.M. Wei, X.T. Huang, J. Solid State Chem. 184 (2011) 578.
[29] M.P. Yeager, D. Su, N.S. Marinkovic, X.W. Teng, J. Electrochem. Soc. 159 (2012) A1598.
[30] X. Xia, D. Chao, Z. Fan, C. Guan, X. Cao, H. Zhang, H.J. Fan, Nano Lett. 14 (2014) 1651.
[31] X.H. Xia, J.P. Tu, Y.Q. Zhang, X.L. Wang, C.D. Gu, X.B. Zhao, H.J. Fan, ACS Nano 6 (2012) 5531.
[32] X. Xia, Y.Q. Zhang, D. Chao, G. Cao, Y. Zhang, L. Li, X. Ge, I.M. Bacho, J. Tu, H.J. Fan, Nanoscale (2014), http://dx.doi.org/10.1039/C4NR00024B.
[33] M.M. Natile, A. Glisenti, Chem. Mater. 14 (2002) 4895.
[34] P. Adelhelm, Y.S. Hu, L. Chuenchom, M. Antonietti, B.M. Smarsly, J. Maier, Adv. Mater. 19 (2007) 4012.
[35] G. Wang, Q. Dong, Z. Ling, C. Pan, C. Yu, J.S. Qiu, J. Mater. Chem. 22 (2012) 21819.
[36] D.D. Han, P.C. Xu, X.Y. Jing, J. Wang, P.P. Yang, Q.H. Shen, J.Y. Liu, D.L. Song, Z. Gao, M.L. Zhang, J. Power Sources 235 (2013) 45.
[37] X.H. Xia, J.P. Tu, Y.J. Mai, R. Chen, X.L. Wang, C.D. Gu, X.B. Zhao, Chem. Eur. J. 17 (2011) 10898.
[38] M.S. Wu, H.H. Hsieh, Electrochim. Acta 53 (2008) 3427.
[39] M.S. Wu, Y.A. Huang, C.H. Yang, H.H. Jow, Int. J. Hydrogen Energy 32 (2007) 4153.
[40] Y.Q. Zhang, X.H. Xia, J.P. Tu, Y.J. Mai, S.J. Shi, X.L. Wang, C.D. Gu, J. Power Sources 199 (2012) 413.
[41] X.Y. Yan, X.L. Tong, J. Wang, C.W. Gong, M.G. Zhang, L.P. Liang, Mater. Lett. 95 (2013) 1.
[42] Y. Gao, S. Chen, D. Cao, G. Wang, J. Yin, J. Power Sources 195 (2010) 1757.
[43] C.Z. Yuan, L.R. Hou, Y.L. Feng, S.L. Xiong, X.G. Zhang, Electrochim. Acta 88 (2013) 507.